International Journal of Heat and Mass Transfer 52 (2009) 3176–3186

Contents lists available at ScienceDirect

International Journal of Heat and Mass Transfer

journal homepage: www.elsevier.com/locate/ijhmt

Numerical investigation of laminar natural convective heat transfer from a horizontal triangular cylinder to its concentric cylindrical enclosure

Xu Xu [a], Gonggang Sun [a], Zitao Yu [b,*], Yacai Hu [b], Liwu Fan [c,*], Kefa Cen [d]

[a] College of Metrology and Measurement Engineering, China Jiliang University, Hangzhou 310018, PR China
[b] Institute of Thermal Science and Power Systems, Zhejiang University, Hangzhou 310027, PR China
[c] Mechanical Engineering Department, Auburn University, 270 Ross Hall, Auburn, AL 36849-5341, USA
[d] State Key Laboratory of Clean Energy Utilization, Zhejiang University, Hangzhou 310027, PR China

ARTICLE INFO

Article history:
Received 6 January 2009
Received in revised form 28 January 2009
Accepted 28 January 2009
Available online 26 March 2009

Submitted to International Journal of Heat and Mass Transfer

Keywords:
Numerical simulation
Laminar flow
Natural convection
Heat transfer
Triangular cylinder
Inclination angle

ABSTRACT

A numerical simulation was conducted to investigate the steady laminar natural convective heat transfer for air within the horizontal annulus between a heated triangular cylinder and its circular cylindrical enclosure. The Boussinesq approximation was applied to model the buoyancy-driven effect and the governing equations were solved using the finite volume method. Four different Rayleigh numbers and four different radius ratios were considered, and four different inclination angles for the inner triangular cylinder were investigated as well. The computed flow and temperature fields were demonstrated in the form of streamlines and isotherms. Variations of the maximum stream function and the local and average Nusselt numbers were displayed as functions of the above-mentioned parameters. Correlations of the average Nusselt number were proposed based on curve fitting. At constant radius ratio, inclination angles of the inner triangular cylinder are found to have negligible effects on the average Nusselt number.

Published by Elsevier Ltd.

1. Introduction

Laminar natural convective heat transfer inside enclosures with internal bodies has been extensively studied in the past decades due to the growing requirement for a deeper understanding of this phenomenon that is related to many industrial applications, including design of solar collectors and thermal storage systems, and thermal management of aviation and consumer electronics as well. As one of the most representative cases, steady laminar natural convection within an annular region constrained between two horizontally placed cylinders has received increased attention. Kuehn and Goldstein [1] presented a review of early works of this subject published before 1970s. In the same paper, an experimental and theoretical study of natural convection between two isothermal horizontal concentric cylinders was also presented. A following paper [2] by the same authors was focused on both concentric and eccentric cylinders and the Rayleigh number range considered was extended. The experimental data reported in these two papers has frequently been referred to as benchmarking results. Since then, a great number of numerical efforts have been made to investigate the steady laminar natural convective heat transfer within horizontal concentric and eccentric circular annuli for different boundary conditions, i.e., isothermal [3–10], constant heat flux [11,12], and mixed boundary conditions [13,14]. The effects of radius ratios, eccentricities, Prandtl numbers [15], and temperature-dependent fluid properties [16] on natural convection have also been studied. Other than the most widely used finite volume approach, some other numerical methods, such as the differential quadrature method [17–19] and the lattice Boltzmann method [20], have been effectively employed in this subject.

Recently, natural convection in horizontal annuli with a non-circular inner or outer cylinder has been studied, including elliptical [21–24], square/rectangular [25,26], rhombic [27,28] cylinders and their combinations. The most concerned combination is a circular cylinder enclosed by a square/rectangular cylinder [29–35]. On the other hand, triangular enclosures in the absence of internal bodies have long been studied for modeling the natural convection heat transfer in pitched roofs [36–38]. However, the authors are unaware of any published work on natural convection in an annulus with an inner triangular cylinder.

Unlike circular or elliptical cylinders, triangular cylinders, due to their asymmetric and piecewise smooth nature, are expected to have special effects on modification of natural convective flow and heat transfer in horizontal annuli. Hence, in order to extend

* Corresponding authors. Tel.: +86 571 87952378; fax: +86 571 87952378 (Z. Yu); tel.: +1 334 844 8386 (L. Fan).
E-mail addresses: yuzitao@zju.edu.cn (Z. Yu), lzf0002@auburn.edu (L. Fan).

0017-9310/$ - see front matter Published by Elsevier Ltd.
doi:10.1016/j.ijheatmasstransfer.2009.01.026

Nomenclature

b	side width of equilateral triangle (m)
c_p	specific heat (kJ/kgK)
g	gravitational acceleration (m/s^2)
h	heat transfer coefficient (W/m^2 K)
k	thermal conductivity (W/mK)
L	characteristic length, $L = R_o - R_i$ (m)
Nu, $\overline{Nu}$	local and average Nusselt number
p, P	dimensional and dimensionless thermodynamic pressure
Pr	Prandtl number
q	local heat flux (W/m^2)
R	radius of circle, (m)
Ra	Rayleigh number
RR	radius ratio, R_o/R_i
s, S	dimensional and dimensionless local coordinate
T, $\overline{T}$	dimensional and dimensionless temperature
u, U	dimensional and dimensionless velocity in x direction
v, V	dimensional and dimensionless velocity in y direction
Greek symbols	
α	thermal diffusivity (m^2/s)
β	thermal expansion coefficient (1/K)
θ	polar coordinate
ν	kinematic viscosity (m^2/s)
ρ	fluid density (kg/m^3)
φ	inclination angle
ψ	dimensionless stream function
Subscripts	
i	inner triangular cylinder
o	outer circular cylinder
L	based on length L
max	maximum

the knowledge of natural convective heat transfer inside horizontal non-circular annuli, the effects of geometric configurations and inclination angles on steady laminar natural convection of air from a triangular cylinder to its concentric cylindrical enclosure are systematically investigated in this study. Equilateral triangular cylinders are only concerned without loss of generality.

The rest of this paper is consisted of four sections. The physical domain of interest and its mathematical formulation are described in the next section. The computational methodology and procedure are then presented, which are followed by a detailed presentation and discussion of the numerical results. Some concluding remarks are finally drawn based on the foregoing analysis.

2. Problem formulation

2.1. Geometric description

The problem to be considered is that of an annular region filled with air between an outer circular cylinder and an inner equilateral triangular cylinder that are concentrically placed. By assuming that both cylinders are extremely long in the axial direction into the page, the problem is considered two-dimensional. The outer and inner cylinders are both isothermal and maintained at constant temperatures T_o and T_i, respectively, with $T_o < T_i$. The physical domain of interest and its associated coordinate systems are sketched in Fig. 1. The problem will be solved in the global Cartesian coordinate with the origin at the center of both the circle and the equilateral triangle. The gravity is set to be along the negative y direction and two special coordinates are adopted to assist the analysis of the numerical results. As shown in Fig. 1, the polar θ coordinate with its origin positioned at the center initiates from the positive y axis (where $\theta = 0$) and rotates in the clockwise direction, whereas the local s coordinate along the triangular walls is adopted with its origin placed at the apex of the triangle (where $s = 0$). It is obvious that the maximum s coordinate is equal to the perimeter of the triangle, $s_{max} = 3b$. The s coordinate is therefore normalized as $S = s/3b$. The inclination angle of the inner triangular cylinder, which is denoted by φ, is also shown in Fig. 1. The radius ratio (RR) is defined as the ratio of the radius of the outer circle to the radius of the circumscribed circle of the inner equilateral triangle, which is expressed as $RR = R_o/R_i$.

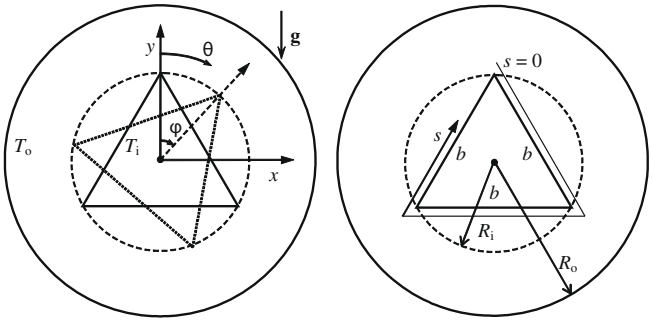

(a) Global coordinates (b) Local coordinate

Fig. 1. Schematic diagram of the physical domain and coordinate systems.

2.2. Governing equations and boundary conditions

A set of dimensionless variables are introduced as:

$$X = \frac{x}{L}, \quad Y = \frac{y}{L}, \quad U = \frac{uL}{\nu}, \quad V = \frac{\nu L}{\nu}, \quad \bar{T} = \frac{T - T_o}{T_i - T_o},$$
$$P = \frac{(p + \rho g y)L^2}{\rho \nu^2}, \quad Pr = \frac{\nu}{\alpha}, \text{ and } Ra = \frac{g\beta(T_i - T_o)L^3}{\nu\alpha},$$

where the characteristic length L is defined as the difference between the radius of the outer circle and the radius of the circumscribed circle of the inner triangle, $L = R_o - R_i$.

By applying these dimensionless variables, the governing equations for this problem in dimensionless form are given by

Continuity:

$$\frac{\partial U}{\partial X} + \frac{\partial V}{\partial Y} = 0, \tag{1}$$

Horizontal direction momentum:

$$U\frac{\partial U}{\partial X} + V\frac{\partial U}{\partial Y} = -\frac{\partial P}{\partial X} + \frac{\partial^2 U}{\partial X^2} + \frac{\partial^2 U}{\partial Y^2}, \tag{2}$$

Vertical direction momentum:

$$U\frac{\partial V}{\partial X} + V\frac{\partial V}{\partial Y} = -\frac{\partial P}{\partial Y} + \frac{\partial^2 V}{\partial X^2} + \frac{\partial^2 V}{\partial Y^2} + \frac{Ra\bar{T}}{Pr}, \tag{3}$$

Energy:

$$U\frac{\partial \bar{T}}{\partial X} + V\frac{\partial \bar{T}}{\partial Y} = \frac{1}{Pr}\left(\frac{\partial^2 \bar{T}}{\partial X^2} + \frac{\partial^2 \bar{T}}{\partial Y^2}\right), \tag{4}$$

where the presence of the last term on the right-hand side of Eq. (3) is due to the application of the Boussinesq approximation.

It is clearly seen that the Prandtl and Rayleigh numbers are the two parameters that govern this problem. Since air is the only concerned fluid, which indicates that the Prandtl number is fixed at $Pr = 0.71$, the effects of the Prandtl number are unavailable in this study. The Rayleigh number, however, is varied within a range up to $Ra = 10^6$, which ensures that the flow is inherently laminar and justifies the steady state assumption. Both hydrodynamic and thermal boundary conditions for this problem are obvious. No-slip boundary conditions hold along both the outer and the inner walls, which are maintained at uniform dimensionless temperatures $\bar{T} = 0$ and $\bar{T} = 1$, respectively.

3. Numerical solution

3.1. Computational details

The governing equations were solved using the finite volume method in which the pressure correction procedure was conducted following the SIMPLE algorithm proposed by Patankar [39]. The grid system was created using unstructured triangular cells, which were unevenly distributed over the computational domain and concentrated near the three vertices of the inner triangle where higher grid densities are required. In discretizing the governing equations, the second order upwind scheme was adopted for both momentum and energy equations, whereas the PRESTO scheme was utilized for pressure correction equation. The convergence criterion was set to 10^{-6} for each variable.

It is worthy noting that in many numerical investigations of natural convection in horizontal annuli, for the sake of symmetry, the problems were solved in half domains and symmetric boundary conditions were set at symmetric planes. In many cases, this simplification successfully saved the computational expenses and was proven to be able to yield fairly good results. However, as discussed by Holtzman et al. [36], though a domain has a symmetric plane along the gravitational direction, the flow and temperature fields may feature asymmetric and the asymmetry becomes more pronounced as the Rayleigh number is increased. Therefore, all cases studied in the present study were solved in entire domains.

3.2. Code validation

Due to the lack of published experimental data for the geometry concerned in the present study, benchmarking results for the horizontal concentric circular annulus by Kehn and Goldstein [1] were used for the validation of the current code. The case of $RR = 2.6$ and $Ra = 4.8 \times 10^4$ was chosen for comparison. The computational domain, thermal properties, and boundary conditions in current code were set to be exactly identical to those in the benchmarking work. The computational procedure, however, was implemented following the way mentioned in the previous section.

The comparison of the equivalent conductivity, which is defined as the ratio of the local Nusselt number to the Nusselt number for pure conduction situation of the same geometry and configuration, is shown in Fig. 2. Along both the outer and the inner walls, most data points exhibit extremely good agreement between the numerical and the benchmarking results, though some little deviations are found at both the lower part of the inner wall and the upper part of the outer wall.

3.3. Grid independence test

To ensure the accuracy of the numerical results and to find a proper size of grids, a grid independence test is carried out in this section for the case of $\varphi = 0°$, $RR = 2.0$, and $Ra = 10^6$. In order to examine the dependence of the computed flow field upon the grid density, the comparison of the maximum dimensionless stream function is presented. As listed in Table 1, various grid numbers yield nearly identical results of the maximum stream function with a maximum deviation less than 4%. Especially, the two greatest grid sizes of 11,000 and 14,000 cells give almost exactly identical results with only a 0.04% deviation. The grid size of about 14 000 cells was therefore chosen for all cases studied.

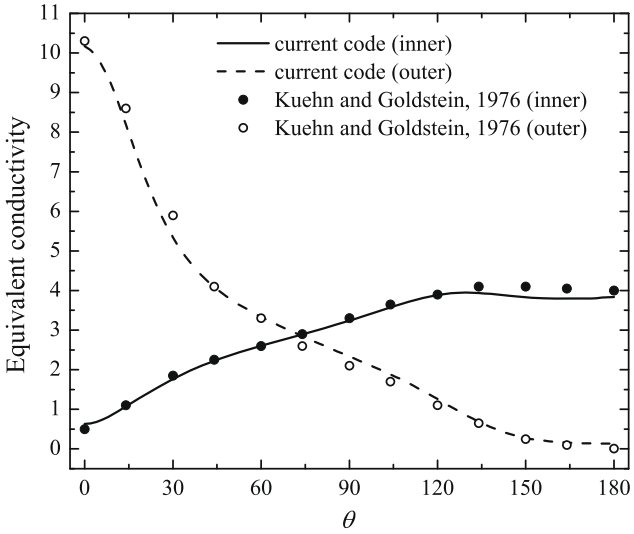

Fig. 2. Comparison of the equivalent conductivity along both the outer and the inner walls between numerical results of current code and available experimental data [1] for a horizontal concentric circular annulus ($RR = 2.6$, $Ra = 4.8 \times 10^4$).

Table 1
Comparison of the maximum stream function among different grid sizes ($RR = 2.0$, $Ra = 10^6$).

Number of cells	ψ_{max}	Deviation (%)
6000	14.5497	3.77
9000	14.3427	2.29
11,000	14.0267	0.04
14,000	14.0213	0.00

4. Results and discussion

The study was first conducted for cases that the apex of the triangle is positioned through the vertical centerline, i.e., $\varphi = 0°$. In these cases, four different radius ratios ($RR = 3.0$, 2.0, 1.5, and 1.2) and four different Rayleigh numbers ($Ra = 10^3$, 10^4, 10^5, and 10^6) were considered. The inner triangular cylinder was then clock wisely rotated about its center for three different angles with increments of 15°, i.e., $\varphi = 15°$, 30°, and 45°. Four radius ratios at $Ra = 10^6$, which is the highest Rayleigh number considered, were studied for each inclination angle.

4.1. Effects of radius ratio and the Rayleigh number at $\varphi = 0°$

4.1.1. Streamlines

A composite diagram of the streamlines for all cases at $\varphi = 0°$ is displayed in Fig. 3, in which the subfigures are arranged going from left to right with ascending Rayleigh number and going down with descending radius ratio. As shown in Fig. 3, the annular domain can be roughly divided into three regions, i.e., two upper regions above the sides of the triangle and the lower region below the bottom of the triangle. In general, the air heated by the triangular wall rises and is then cooled down and falls along the outer circular

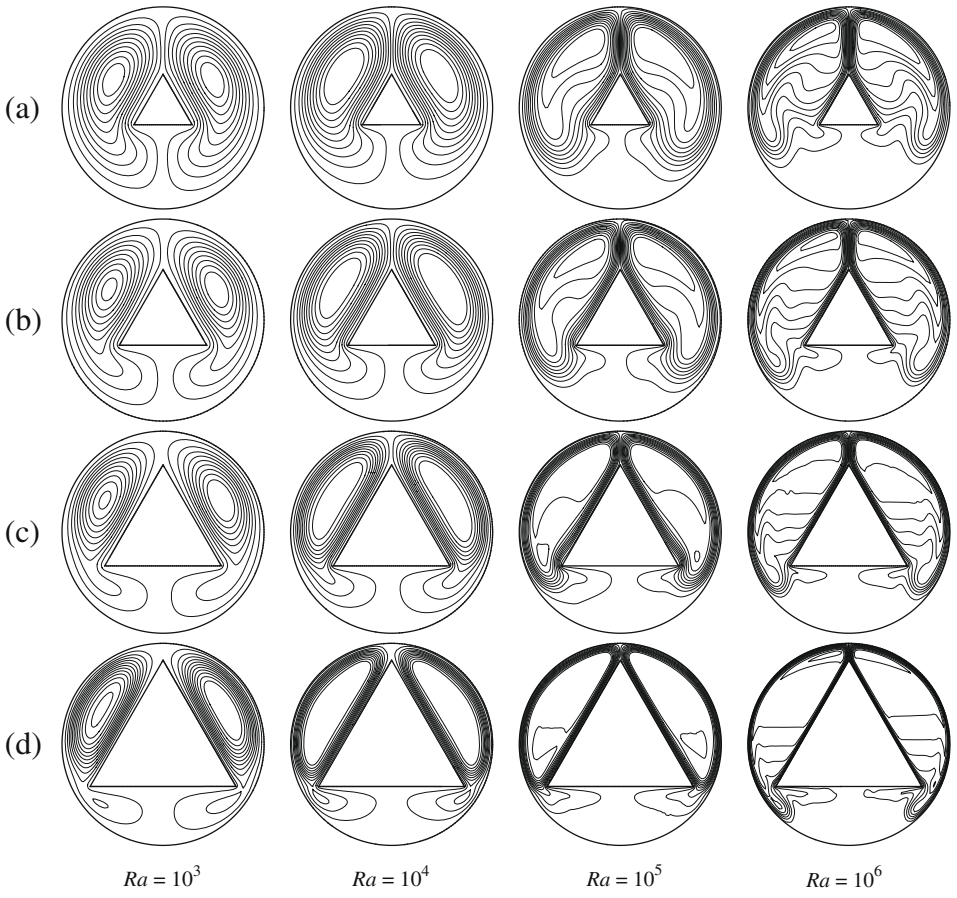

Fig. 3. Streamlines for (a) $RR = 3.0$, (b) $RR = 2.0$, (c) $RR = 1.5$, and (d) $RR = 1.2$ at different Rayleigh numbers.

enclosure, thus leading to a main recirculating cell in each upper region. It is also clearly shown that streamlines are distorted near the two lower vertices of the triangle and the distortion becomes more remarkable with decreasing radius ratio. At $RR = 1.2$, it is observed that each main cell is separated into two vortex cores by strong distortion. In addition, as the Rayleigh number is increased, for each radius ratio the streamlines become more concentrated next to the walls.

The cell patterns exhibit nearly symmetric features about the central planes but show great discrepancies in shape among different Rayleigh numbers. The subfigures in the first two columns in Fig. 3 demonstrate bean-shaped cells. However, the cell patterns for $Ra = 10^5$ and 10^6 are totally different from those for $Ra = 10^3$ and 10^4 because the stronger stretching effect yields more stratified streamlines. At $RR = 1.2$ and $Ra = 10^6$, the streamlines in the middle regions are nearly flat.

4.1.2. Maximum stream function

The maximum stream function, which represents the flow intensity, is compared in Fig. 4. As the radius ratio is deceased, the maximum stream function becomes greater, which is indicative that the flow recirculates faster. This is also proven by the more densely packed streamlines for higher Rayleigh numbers shown in Fig. 3. Because the Rayleigh number in this study is defined based on the gap L between two cylinders, at constant Rayleigh number the flow area for a higher radius ratio is greater than that for a lower radius ratio, thus enhancing the total heat transfer and buoyancy-driven convection. On the other hand, as pointed out by Moukalled and Acharya [30], a competing effect that is produced by increasing the flow area will slow the flow down due to the additional viscous friction. Consequently, the counteraction between these two effects will determine to what extent the recirculating flows are enhanced.

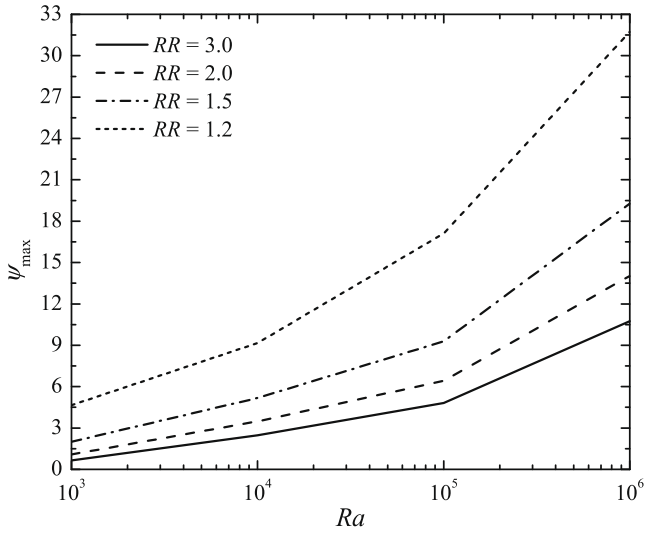

Fig. 4. Variation of the maximum stream function as a function of the Rayleigh number.

At $Ra = 10^3$, the flow enhancement owing to the buoyancy-driven effect compensates for the additional viscous attenuation, which leads to that the maximum stream functions are very close for different radius ratios. However, at higher Rayleigh numbers,

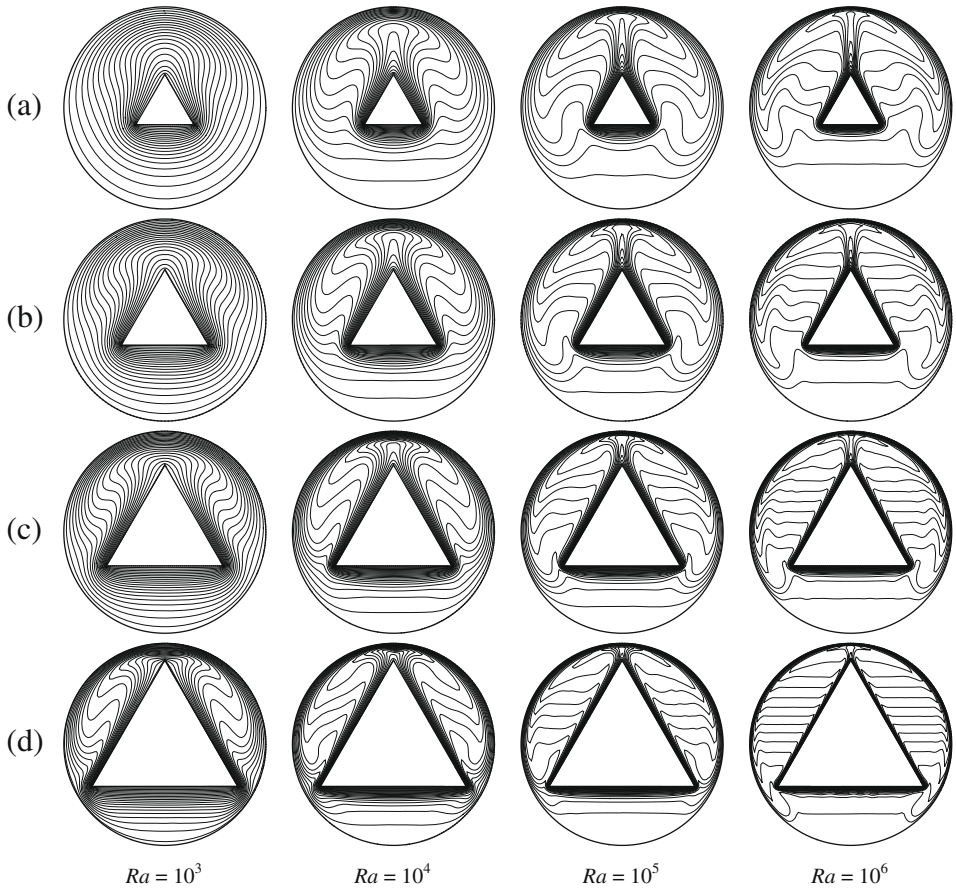

Fig. 5. Isotherms for (a) $RR = 3.0$, (b) $RR = 2.0$, (c) $RR = 1.5$, and (d) $RR = 1.2$ at different Rayleigh numbers.

the maximum stream functions for lower radius ratios increase faster since the buoyancy-driven convection enhancement is dominant and the additional viscous effect becomes insignificant.

4.1.3. Isotherms

The isotherms for various radius ratios and Rayleigh numbers are presented in Fig. 5 as a composite diagram with the same arrangement as Fig. 3. Almost exact symmetry is observed in all subfigures. As the Rayleigh number is increased, the isotherms next to the walls become more densely packed, which indicates higher local heat transfer coefficients. At $Ra = 10^3$ and $RR = 3.0$, the isotherms are nearly concentric circles with little distortion near the apex of the triangle. It turns out that the temperature field is similar to the pure conduction situation due to the weak recirculation in this case.

It is clearly shown in the subfigures for higher Rayleigh numbers that the thermal boundary layer along the inner heated cylinder separate away from the surface near the apex and then form a thermal plume pointing to the top region of the outer cylinder. Another remarkable phenomenon is the stratification in temperature fields, which is more clearly observed with decreasing radius ratio and with increasing Rayleigh number. At $Ra = 10^6$ and $RR = 1.2$, the isotherms are almost flat and uniformly distributed along the vertical direction.

4.1.4. Local Nusselt number

The local Nusselt number based on the characteristic length L is defined as

$$Nu_L = \frac{hL}{k}, \tag{5}$$

where the heat transfer coefficient h is evaluated by

$$h = \frac{q}{T_i - T_o}, \tag{6}$$

where q is the local heat flux along the outer and the inner walls.

Fig. 6 depicts the variation of the local Nusselt number along the outer circular wall. As expected, the relatively flat solid curves, which correspond to the cases of $Ra = 10^3$, are much lower than other curves. The local Nusselt numbers become much greater in the upper regions of the annuli with increasing Rayleigh number for each radius ratio, because of the increasing convection contribution to heat transfer. In most cases with higher local Nusselt numbers, two peaks are observed around the top points ($\theta = 0^\circ$ or 360°) due to the thermal plumes that are observed in Fig. 5. The distance between the two peak positions is identical to the width of the thermal plume. When the thermal plume is very weak for some cases, the two peaks merge into one peak which is right at the top point. At $Ra = 10^6$, the highest peak value is found for $RR = 1.5$. It is also shown that in the lower regions ($120^\circ < \theta < 240^\circ$), the local Nusselt numbers are always low due to the fact that conduction in the lower regions is dominant.

The variation of the local Nusselt number along the inner triangular wall is displayed in Fig. 7. Two peaks right at the two lower vertices of the triangle ($S = 1/3$ and $2/3$) are observed. The peak values decrease with decreasing radius ratio and with decreasing Rayleigh number. In the two upper regions ($0 \leqslant S \leqslant 1/3$ and $2/3 \leqslant S \leqslant 1$), the curves are more linear for $RR = 1.2$ than for other radius ratios due to stronger thermal stratification. In the conduction-dominated lower regions ($1/3 \leqslant S \leqslant 2/3$), the curves are flat as expected. At the apexes ($S = 0$ or 1), the curves exhibit local peaks for the cases with lower Rayleigh numbers. However, at higher Rayleigh numbers, these local peaks switch to local troughs due to the presence of thermal plumes. Recall that the thermal plume

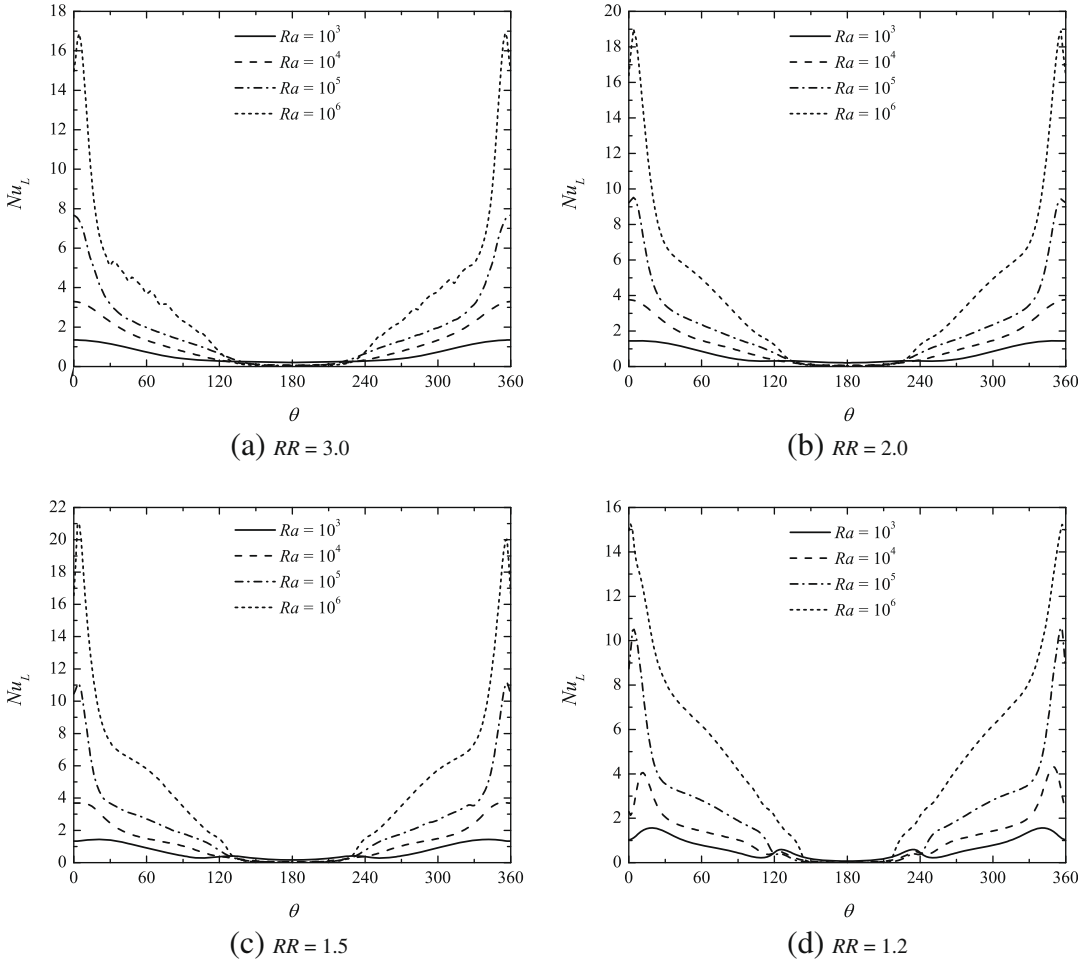

Fig. 6. Variation of the local Nusselt number along the outer circular wall.

is formed by the separated thermal boundary layers near the apex. Stronger thermal plume formation at higher Rayleigh numbers indicates more intensive separation of boundary layers, thus leading to lower local heat transfer rates.

4.1.5. Average Nusselt number and correlation

The variation of the average Nusselt number that is utilized to evaluate the overall heat transfer rate is presented in this section. The average Nusselt numbers along the outer and the inner walls are defined, respectively, as

$$\overline{Nu_L} = \frac{1}{2\pi}\int_0^{2\pi} Nu_L\, d\theta, \tag{7}$$

$$\overline{Nu_L} = \frac{1}{3b}\int_0^{3b} Nu_L\, ds = \int_0^1 Nu_L\, dS. \tag{8}$$

The average Nusselt numbers for all cases studied are plotted in Fig. 8. For both the outer and the inner walls, the average Nusselt number increases as the Rayleigh number is increased due to the increasing contribution of natural convection. The radius ratio, however, has opposite influences on the outer and inner walls. It is shown that increasing radius ratio decreases the average Nusselt number along the outer wall, and on the contrary, increasing radius ratio increases the average Nusselt number along the inner wall. For the average Nusselt number along the outer wall, the influence of the radius ratio at lower Rayleigh numbers is insignificant, and as the Rayleigh number increases the influence becomes remarkable.

Instead of using the characteristic length L, the Nusselt numbers along the outer and the inner walls can be defined based on their respective perimeters, $2\pi R_o$ and $3b$, as

$$Nu_o = \frac{2\pi R_o h}{k}, \tag{9}$$

$$Nu_i = \frac{3bh}{k} = \frac{3\sqrt{3}R_i h}{k}. \tag{10}$$

It is evident that at steady state the average Nusselt numbers along the outer and inner walls are identical to each other, i.e., $\overline{Nu} = \overline{Nu_o} = \overline{Nu_i}$, so there is no need to distinguish them. The average Nusselt numbers based on the definitions from either Eq. (9) or Eq. (10) are calculated and plotted in Fig. 9. At constant radius ratio, the four points on the log-log coordinates, $\log(\overline{Nu})$ vs $\log(Ra)$, are nearly along a straight line. By performing curve fitting via a least square regression method, the linear expressions for the four lines are found as shown in Fig. 9. The correlations of the average Nusselt number are then obtained and listed in Table 2. Note that the correlations are only valid under the laminar flow condition and at $Pr = 0.71$. It is seen that the exponent of the Rayleigh number increases with decreasing radius ratio and all exponents lie in the range between 0.24 and 0.29, which is consistent with the exponent range from 0.23 to 0.3 that is reported in available literature for laminar natural convective heat transfer in horizontal annuli with other geometries.

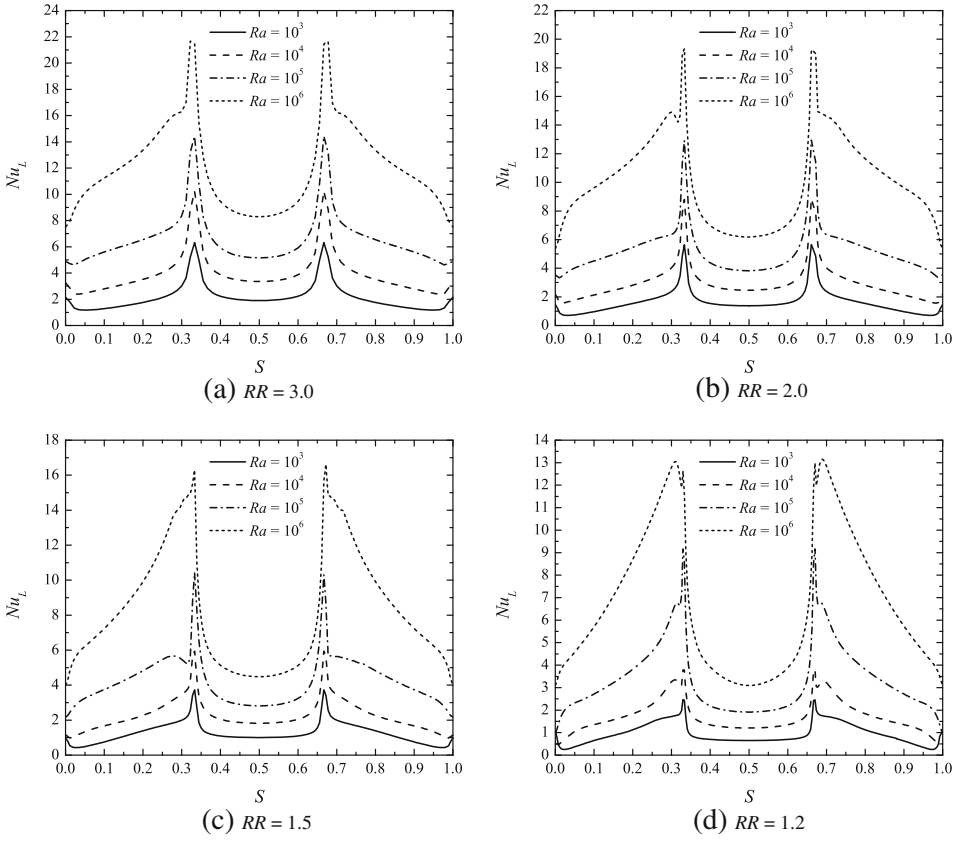

Fig. 7. Variation of the local Nusselt number along the inner triangular wall.

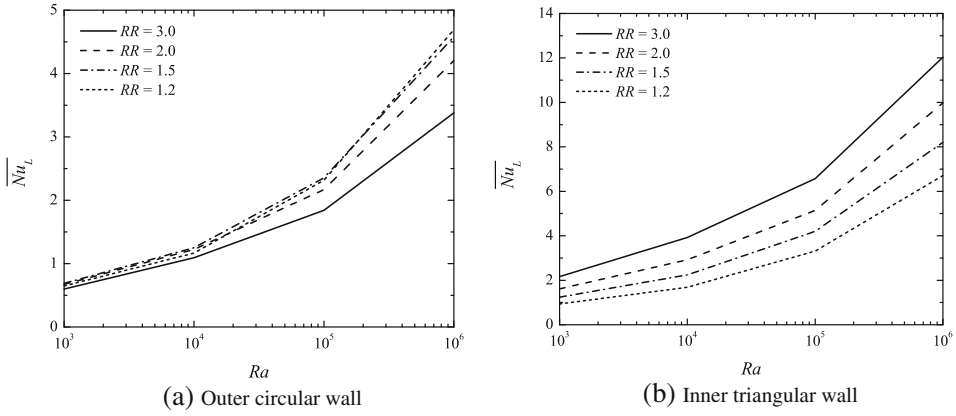

Fig. 8. Variation of the average Nusselt number along both the (a) outer and the (b) inner walls.

4.2. Effects of inclination angle at Ra = 10^6

4.2.1. Streamlines

A composite diagram of the streamlines for all cases at $Ra = 10^6$ is displayed in Fig. 10, in which the subfigures are arranged going from left to right with ascending inclination angle and going down with descending radius ratio. The most evident feature in these subfigures is that the appearance of strongly asymmetric flow patterns when the inner triangle is rotated. This is due to that the symmetric plane of the domain of interest is no longer along the gravitational direction after being rotated. Once the inner cylinder is rotated, no matter what the inclination angle is, the main recirculating cell in the left upper region separates into at least two vortex cores. As the radius ratio is lowered, the influence of the inclination angle becomes more remarkable. The boundary layer separation is clearly seen for higher inclination angles, which occurs near the left vertex of the triangle. The separated boundary layer reattaches to the left side wall, which produces a small recirculating cell. As the inclination angle is increased and as the radius ratio is decreased, the boundary layer separation becomes more pronounced and those small cells become bigger. Multicellular flow patterns appear when the inclination angle is larger than 30°. At $\varphi = 45°$ and $RR = 1.2$, four cells related to the Rayleigh–Benard convection are clearly observed in the upper region. It is worthy noting that if the inclination angle is further increased to 60°, that is the case of the vertical side on the top, the flow becomes unstable. In the present study, cases without steady solutions were not considered.

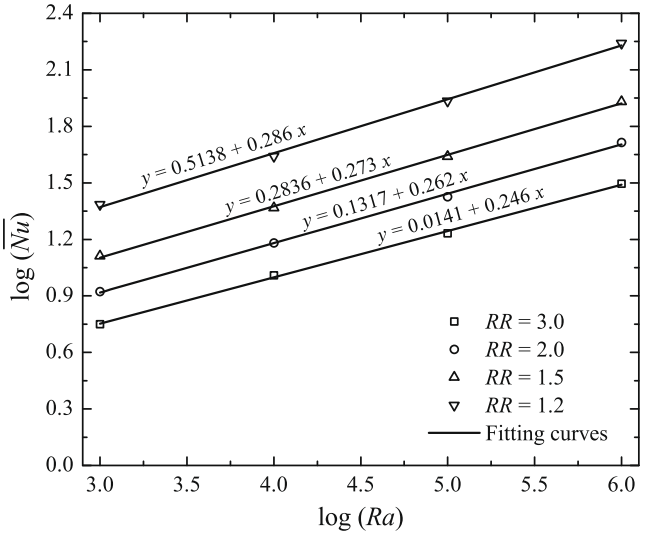

Fig. 9. Curve fitting of the average Nusselt number as a function of the Rayleigh number.

4.2.2. Isotherms

The isotherms for various radius ratios and inclination angles are displayed in Fig. 11 as a composite diagram with the same arrangement as Fig. 10. Once the triangular cylinder is rotated, the thermal plume is also turned in the same direction but with smaller angles. In many cases, strong thermal stratification still exists. However, at higher inclination angles, stratification in the left upper regions is broken due to the presence of multicellular flow patterns observed in Fig. 10. An interesting phenomenon is that, at $RR = 1.2$ and $\varphi = 45°$, due to the presence of the Rayleigh–Benard cells, a secondary thermal plume appears ascending from the upper half of the left side wall of the triangle.

Table 2
Correlations of the average Nusselt number based on curve fitting.

RR	$\overline{Nu}$	Maximum deviation (%)
3.0	$1.033\ Ra^{0.246}$	2.81
2.0	$1.354\ Ra^{0.262}$	3.71
1.5	$1.921\ Ra^{0.273}$	2.02
1.2	$3.264\ Ra^{0.286}$	4.04

4.2.3. Local and average Nusselt numbers

The local Nusselt number along the outer circular wall for different radius ratios is shown in Fig. 12. In general, the maximum values are not affected by the inclination angle. The peak positions, however, are altered by the rotation of the triangular cylinder. In Fig. 13, the local Nusselt numbers along the inner triangular wall for different radius ratios are plotted. Since the local dimensionless S coordinate is attached to the walls of the triangle, the two peak positions for each case are fixed at $S = 1/3$ (right vertex) and $S = 2/3$ (left vertex). The most remarkable influence of the inclination angle is the alternation of the peak values. At the right vertex, the rotation of the triangular cylinder strongly enhances the local Nusselt number, whereas at the left vertex, the inverse effect is observed. At constant radius ratio, however, though the local Nusselt number is nearly everywhere higher for a greater inclination angle, the peak

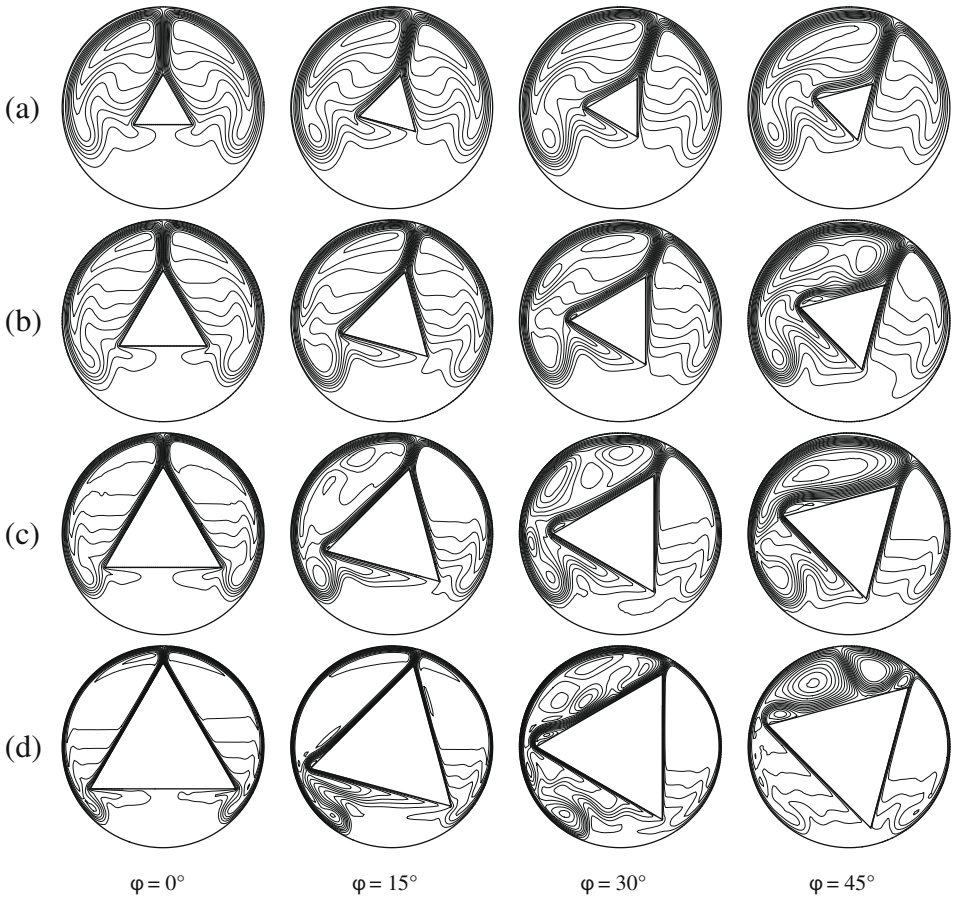

Fig. 10. Streamlines for (a) $RR = 3.0$, (b) $RR = 2.0$, (c) $RR = 1.5$, and (d) $RR = 1.2$ at different inclination angles at $Ra = 10^6$.

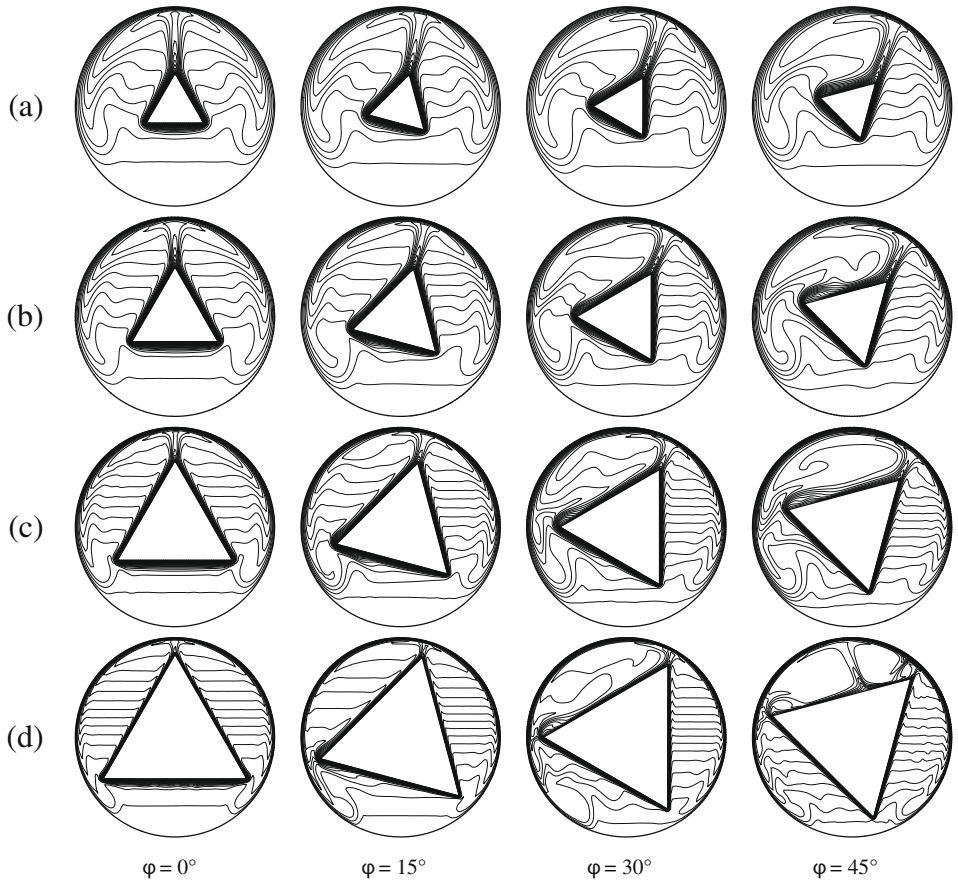

Fig. 11. Isotherms for (a) $RR = 3.0$, (b) $RR = 2.0$, (c) $RR = 1.5$, and (d) $RR = 1.2$ at different inclination angles at $Ra = 10^6$.

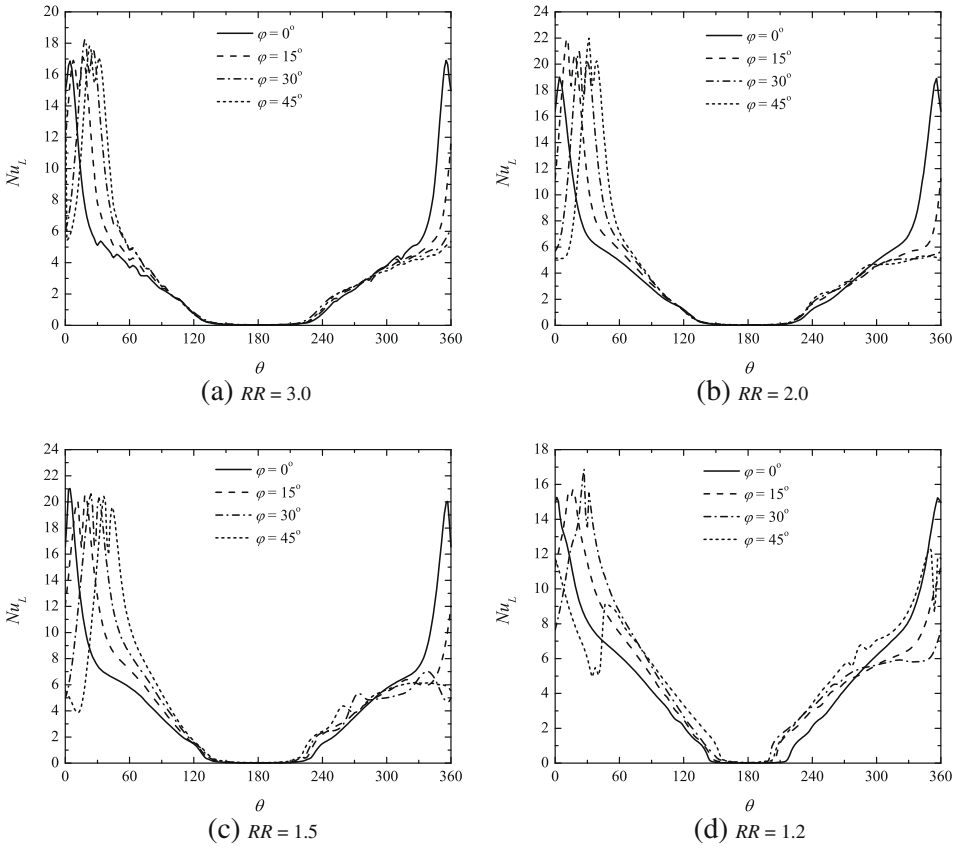

Fig. 12. Variation of the local Nusselt number along the outer circular wall for different radius ratios at $Ra = 10^6$.

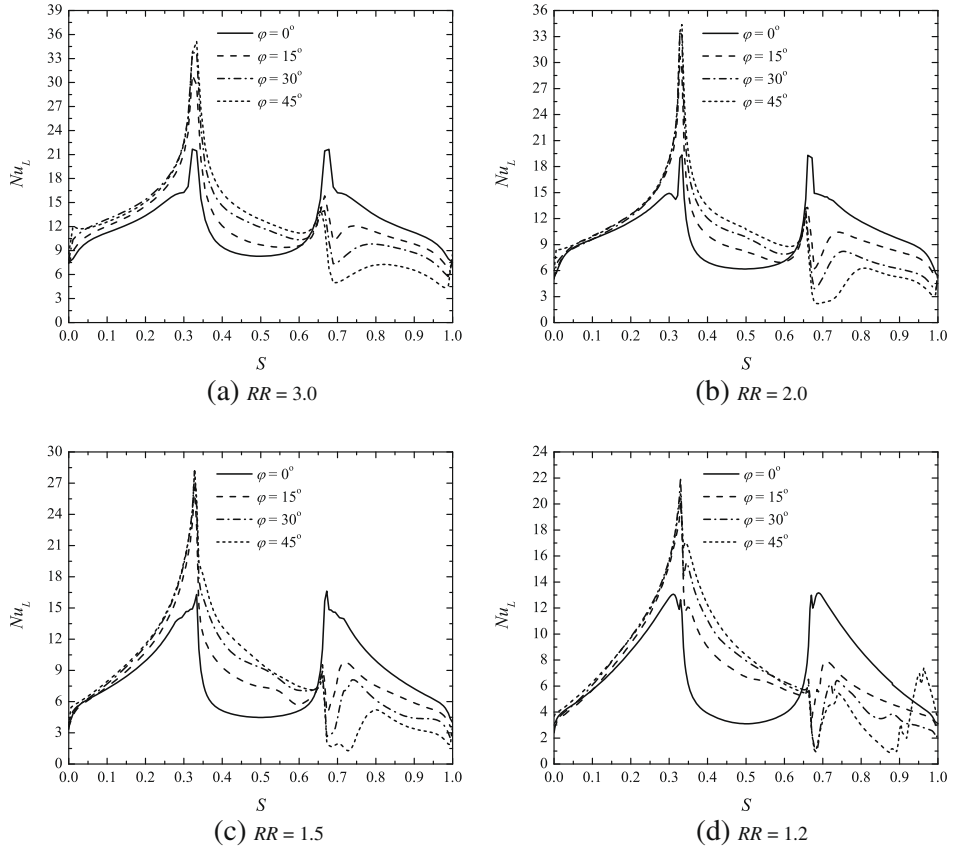

Fig. 13. Variation of the local Nusselt number along the inner triangular wall for different radius ratios at $Ra = 10^6$.

values are almost identical for all angles. An evident local trough is observed on the curve of $RR = 1.2$ and $\varphi = 45^\circ$ within the range of $2/3 \leqslant S \leqslant 1$. According to the foregoing discussion, the presence of a thermal plume yields a trough in the local Nusselt number curve due to the thermal boundary layer separation. Therefore, the local trough observed here directly proves the presence of the Rayleigh-Benard cells and the induced secondary thermal plume.

Finally, variations of the average Nusselt number for different radius ratios are demonstrated in Fig. 14. The four nearly flat curves indicate that the inclination angles have negligible effects on the average Nusselt number. Though the presence of multicellular flow patterns remarkably alters the local heat transfer along both the outer and the inner walls, the overall heat transfer rate within the domain of interest is not affected and remains nearly constant with increasing inclination angle.

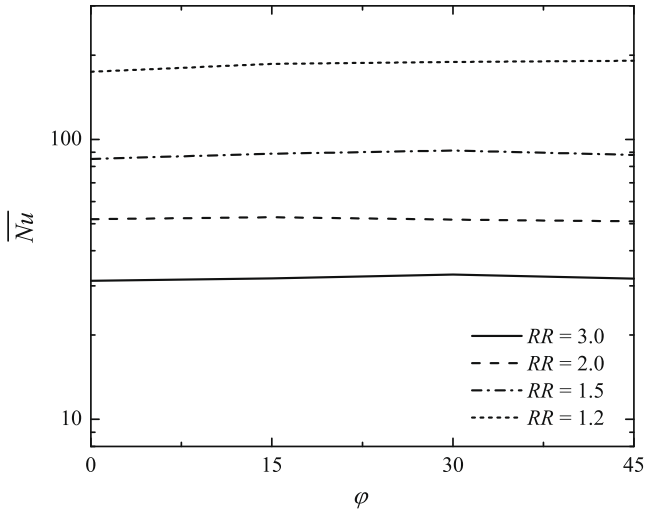

Fig. 14. Variation of the average Nusselt number for different inclination angles at $Ra = 10^6$.

5. Conclusions

A numerical investigation of steady laminar natural convection from a heated triangular cylinder to its circular cylindrical enclosure was presented. Based on the foregoing analysis of the numerical results, some concluding remarks can be drawn as follows:

1. The formation of thermal plumes was clearly observed at higher Rayleigh numbers due to the thermal boundary layer separation. Another remarkable phenomenon is the thermal stratification, which becomes stronger with decreasing radius ratio and with increasing Rayleigh number.

2. At constant radius ratio, due to the increasing convection contribution to heat transfer, the local Nusselt numbers along both the outer and the inner walls are increased with increasing Rayleigh number.

3. Correlations of the average Nusselt number for different radius ratios were proposed. The exponent of the Rayleigh number increases with decreasing radius ratio and all exponents lie in the range between 0.24 and 0.29.

4. Multicellular flow patterns appear at larger inclination angles. At $\varphi = 45^\circ$ and $RR = 1.2$, four recirculating cells related to the Rayleigh–Benard convection can be seen in the upper region, which result in a secondary thermal plume.

5. The peak positions on the curves of the local Nusselt number along the outer wall are altered by the rotation of the inner

triangular cylinder because the thermal plumes are turned also. At constant radius ratio, however, it is found that the inclination angles have negligible effects on the average Nusselt number.

Acknowledgements

The financial support provided by the National Science Foundation of China (NSFC) through Grant No. 50706044 is gratefully acknowledged. The third author (Z.T. Yu) would like to express his appreciation for a grant from the Program of Outstanding Young Scholars of Zhejiang University (Zijin Program).

References

[1] T.H. Kuehn, R.J. Goldstein, An experimental and theoretical study of natural convection in the annulus between horizontal concentric cylinders, Journal of Fluid Mechanics 74 (1976) 695–719.
[2] T.H. Kuehn, R.J. Goldstein, An experimental study of natural convection heat transfer in concentric and eccentric horizontal cylindrical annuli, ASME Journal of Heat Transfer 100 (1978) 635–640.
[3] U. Projahn, H. Rieger, H. Beer, Numerical analysis of laminar natural convection between concentric and eccentric cylinders, Numerical Heat Transfer, Part B: Fundamentals 4 (1981) 131–146.
[4] C.H. Cho, K.S. Chang, K.H. Park, Numerical simulation of natural convection in concentric and eccentric horizontal cylindrical annuli, ASME Journal of Heat Transfer 104 (1982) 624–630.
[5] M.A. Hessami, A. Pollard, R.D. Rowe, Numerical calculations of natural convection heat transfer between horizontal concentric isothermal cylinders–effects of variation of fluid properties, ASME Journal of Heat Transfer 106 (1984) 668–671.
[6] A.W. Date, Numerical prediction of natural convection heat transfer in horizontal annulus, International Journal of Heat and Mass Transfer 29 (1986) 1457–1464.
[7] D.N. Mahony, R. Kumar, E.H. Bishop, Numerical investigation of variable property effects on laminar natural convection of gases between two horizontal isothermal concentric cylinders, ASME Journal of Heat Transfer 108 (1986) 783–789.
[8] J.S. Yoo, J.Y. Choi, M.U. Kim, Multicellular natural convection of a low Prandtl number fluid between horizontal concentric cylinders, Numerical Heat Transfer, Part A: Applications 25 (1994) 103–115.
[9] G. Guj, F. Stella, Natural convection in horizontal eccentric annuli: numerical study, Numerical Heat Transfer, Part A: Applications 27 (1995) 89–105.
[10] J.D. Chung, C.J. Kim, H. Yoo, J.S. Lee, Numerical investigation on the bifurcative natural convection in a horizontal concentric annulus, Numerical Heat Transfer, Part A: Applications 36 (1999) 291–307.
[11] E.K. Glakpe, C.B. Watkins, J.N. Cannon, Constant heat flux solutions for natural convection between concentric and eccentric horizontal cylinders, Numerical Heat Transfer, Part A: Applications 10 (1986) 279–295.
[12] J.S. Yoo, Dual free-convective flows in a horizontal annulus with a constant heat flux wall, International Journal of Heat and Mass Transfer 46 (2003) 2499–2503.
[13] R. Kumar, Study of natural convection in horizontal annuli, International Journal of Heat and Mass Transfer 31 (1988) 1137–1148.
[14] C.J. Ho, Y.H. Lin, T.C. Chen, A numerical study of natural convection in concentric and eccentric horizontal cylindrical annuli with mixed boundary conditions, International Journal of Heat and Fluid Flow 10 (1989) 40–47.
[15] U. Projahn, H. Beer, Prandtl number effects on natural convection heat transfer in concentric and eccentric horizontal cylindrical annuli, Heat and Mass Transfer 19 (1985) 249–254.
[16] F. Shahraki, Modeling of buoyancy-driven flow and heat transfer for air in a horizontal annulus: effects of vertical eccentricity and temperature-dependent properties, Numerical Heat Transfer, Part A: Applications 42 (2002) 603–621.
[17] C. Shu, Application of DQ method to simulate natural convection in a concentric annulus, International Journal for Numerical Methods in Fluids 30 (1999) 977–993.
[18] C. Shu, K.S. Yeo, Q. Yao, An efficient approach to simulate natural convection in arbitrarily eccentric annuli by vorticity-stream function formulation, Numerical Heat Transfer, Part A: Applications 38 (2000) 739–756.
[19] T.S. Lee, G.S. Hu, C. Shu, Application of GDQ method for the study of natural convection in horizontal eccentric annuli, Numerical Heat Transfer, Part A: Applications 41 (2002) 803–815.
[20] Y. Peng, Y.T. Chew, C. Shu, Numerical simulation of natural convection in a concentric annulus between a square outer cylinder and a circular inner cylinder using the Taylor-series-expansion and least-squares-based lattice Boltzmann method, Physical Review E 67 (2003) 026701. p. 6.
[21] M.M. Elshamy, M.N. Ozisik, J.P. Coulter, Correlation for laminar natural convection between confocal horizontal elliptical cylinders, Numerical Heat Transfer, Part A: Applications 18 (1990) 95–112.
[22] C.H. Cheng, C.C. Chao, Numerical prediction of the buoyancy-driven flow in the annulus between horizontal eccentric elliptical cylinders, Numerical Heat Transfer, Part A: Applications 30 (1996) 283–303.
[23] Y.D. Zhu, C. Shu, J. Qiu, J. Tani, Numerical simulation of natural convection between two elliptical cylinders using DQ method, International Journal of Heat and Mass Transfer 47 (2004) 797–808.
[24] M. Djezzar, M. Daguenet, Natural steady convection in a space annulus between two elliptic confocal ducts, ASME Journal of Applied Mechanics 73 (2006) 88–95.
[25] H. Asan, Natural convection in an annulus between two isothermal concentric square ducts, International Communications in Heat and Mass Transfer 27 (2000) 367–376.
[26] A. Kumar De, A. Dalal, A numerical study of natural convection around a square, Horizontal, heated cylinder placed in an enclosure, International Journal of Heat and Mass Transfer 49 (2006) 4608–4623.
[27] F. Moukalled, H. Diab, S. Acharya, Laminar natural convection in a horizontal rhombic annulus, Numerical Heat Transfer, Part A: Applications 24 (1993) 89–107.
[28] F. Moukalled, S. Acharya, Laminar natural convection heat transfer in an eccentric rhombic annulus, Numerical Heat Transfer, Part A: Applications 26 (1994) 551–568.
[29] N.K. Ghaddar, Natural convection heat transfer between a uniformly heated cylindrical element and its rectangular enclosure, International Journal of Heat and Mass Transfer 35 (1992) 2327–2334.
[30] F. Moukalled, S. Acharya, Natural convection in the annulus between concentric horizontal circular and square cylinders, AIAA Journal of Thermophysics and Heat Transfer 10 (1996) 524–531.
[31] G. Cesini, M. Paroncini, G. Cortellab, M. Manzan, Natural convection from a horizontal cylinder in a rectangular cavity, International Journal of Heat and Mass Transfer 42 (1999) 1801–1811.
[32] C. Shu, H. Xue, Y.D. Zhu, Numerical study of natural convection in an eccentric annulus between a square outer cylinder and a circular inner cylinder using DQ method, International Journal of Heat and Mass Transfer 44 (2001) 3321–3333.
[33] C. Shu, Y.D. Zhu, Efficient computation of natural convection in a concentric annulus between an outer square cylinder and an inner circular cylinder, International Journal for Numerical Methods in Fluids 38 (2002) 429–445.
[34] H. Ding, C. Shu, K.S. Yeo, Z.L. Lu, Simulation of a natural convection in eccentric annuli between a square outer cylinder and a circular inner cylinder using a local MQ-DQ method, Numerical Heat Transfer, Part A: Applications 47 (2005) 291–313.
[35] B.S. Kim, D.S. Lee, M.Y. Ha, H.S. Yoon, A numerical study of natural convection in a square enclosure with a circular cylinder at different vertical locations, International Journal of Heat and Mass Transfer 51 (2008) 1888–1906.
[36] G.A. Holtzman, R.W. Hill, K.S. Ball, Laminar natural convection in isosceles triangular enclosures heated from below and symmetrically cooled from above, ASME Journal of Heat Transfer 122 (2000) 485–491.
[37] H. Asan, L. Namli, Laminar natural convection in a pitched roof of triangular cross-section: summer day boundary conditions, Energy and Buildings 33 (2000) 69–73.
[38] H. Asan, L. Namli, Numerical simulation of buoyant flow in a roof of triangular cross-section under winter day boundary conditions, Energy and Buildings 33 (2001) 753–757.
[39] S.V. Patankar, Numerical Heat Transfer and Fluid Flow, Hemisphere Publishing Corporation, Washington, DC, 1980. pp. 126–130.